A spectral hole memory for light at the single photon level

Kutlu Kutluer,[1] María Florencia Pascual-Winter,[2] Julian Dajczgewand,[3] Patrick M. Ledingham,[1,*] Margherita Mazzera,[1,†] Thierry Chanelière,[3] and Hugues de Riedmatten[1,4]

[1] *ICFO-Institut de Ciencies Fotoniques, Mediterranean Technology Park, 08860 Castelldefels (Barcelona), Spain*
[2] *Laboratorio de Fotónica y Optoelectrónica, Centro Atómico Bariloche and Instituto Balseiro, C.N.E.A., (8400) San Carlos de Bariloche, Argentina*
[3] *Laboratoire Aimé Cotton UMR 9188, CNRS, Université Paris-Sud and ENS Cachan, Bâtiment 505, Campus Universitaire, 91405 Orsay, France*
[4] *ICREA-Institució Catalana de Recerca i Estudis Avançats, 08015 Barcelona, Spain*

(Dated: September 11, 2015)

We demonstrate a solid state spin-wave optical memory based on stopped light in a spectral hole. A long lived narrow spectral hole is created by optical pumping in the inhomogeneous absorption profile of a Pr^{3+}:Y_2SiO_5 crystal. Optical pulses sent through the spectral hole experience a strong reduction of their group velocity and are spatially compressed in the crystal. A short Raman pulse transfers the optical excitation to the spin state before the light pulse exits the crystal, effectively stopping the light. After a controllable delay, a second Raman pulse is sent, which leads to the emission of the stored photons. We reach storage and retrieval efficiencies for bright pulses of up to 39 % in a 5 mm-long crystal. We also show that our device works at the single photon level by storing and retrieving 3 μs-long weak coherent pulses with efficiencies up to 31 %, demonstrating the most efficient spin-wave solid state optical memory at the single-photon level so far. We reach an unconditional noise level of $(9 \pm 1) \times 10^{-3}$ photons per pulse in a detection window of 4 μs leading to a signal-to-noise ratio of 33 ± 4 for an average input photon number of 1, making our device promising for long-lived storage of non-classical light.

PACS numbers: 03.67.Hk,42.50.Gy,42.50.Md

Coherent interactions between light and atoms play an important role in modern quantum science [1]. They enable the control of the properties of light, e.g. its velocity, until the extreme case where the light is stopped. This allows the realization of quantum memories for light, which are fundamental building blocks of complex quantum information processing protocols [2–6]. The implementation of a quantum memory for light requires the mapping of a single photon light field onto long-lived atomic coherence.

Rare-earth doped solids are attractive for quantum memory applications because they contain a large number of naturally trapped atoms with long spin and optical coherence times. Several experiments have demonstrated the storage of quantum information carried by weak coherent light states in the optically excited state of rare-earth ions using the atomic frequency comb (AFC) [7–12] or gradient echo memory (GEM) technique [13, 14]. Non-classical states of light have also been stored in excited states using AFC [15–19]. However, the storage in the excited state leads to short and mostly predetermined storage times. Longer storage times and on-demand read-out can be achieved by transfering the optical collective excitation into spin collective excitations (spin waves) using strong Raman pulses [20, 21]. AFC spin-wave storage has been extended to the quantum regime recently [22, 23], with storage and retrieval efficiencies of a few percents.

Another well-known technique for quantum storage is based on Electromagnetically-Induced Transparency (EIT) [24–27]. It relies on the creation of a narrow transparency window in an otherwise opaque medium, thanks to the application of a control field. Stopped light based on EIT has also been demonstrated in rare-earth doped crystals (Pr^{3+}:Y_2SiO_5) [28], leading (together with dynamical decoupling techniques) to ultra-long storage time for bright pulses [29], up to the regime of one minute [30], the longest light storage time demonstrated so far in any system. However, the efficiency for these experiments was also quite low (few percent at most). Moreover EIT has not yet been demonstrated at the single photon level in doped crystals. This may prove challenging, because of the noise induced by the control field during the read-out.

In this Letter, we demonstrate a simple and robust alternative protocol to store and retrieve light in the spin-state of a doped crystal, that enables us to reach high efficiencies and single photon level operation. The technique, proposed by Lauro et al. [31], uses a permanent transparency window created in a doped crystal by spectral hole burning. While the protocol is similar to EIT because it is based on slow light, there are two important differences. First, the transparency window is not created dynamically with a control pulse, but is created by optical pumping way before the photons to be stored enters the medium. Second, the photons will excite optical coherence with off resonance atoms. There is therefore no dark-state as in EIT. The storage mechanism is then based on the sequential conversion of this optical coherence into a spin coherence, using short Raman π pulses. This is important in practice because the Raman pulses

can be much shorter than the retrieved single photon, which enables temporal filtering . This greatly facilitates the operation at the single-photon level. Thanks to the robust memory preparation, we demonstrate storage and retrieval efficiencies up to 39 % for bright pulses. In addition, we demonstrate the spin-wave storage and retrieval of weak coherent pulses at the sub-photon level with an efficiency of 31 %, the highest achieved so far for a single-photon level solid state spin-wave optical memory [22, 23]. We reach an unconditional noise floor of $(2.25 \pm 0.25) \times 10^{-3}$ photons/μs. For a detection window of 4 μs, this leads to a signal-to-noise ratio of 33 ± 4 for an average input photon number of 1 (together with a slightly reduced efficiency of 23 %), the highest demonstrated so far in a crystal. Our experiment shows that optical storage based on spectral holes can work in the quantum regime.

The experimental setup is shown in Fig. 1(a). The source of coherent light at 606 nm is a Toptica TA-SHG-pro laser, frequency stabilized by means of the Pound-Drevel-Hall technique with a home-madeFabry-Perot cavity in vacuum. Before the memory, it is split into two beams, one used as input beam (150 μW of power and diameter of 70 μm, at the memory crystal) and the other (20 mW of power and diameter of 300 μm, at the memory crystal) employed for the memory preparation and for the Raman pulses. Both are frequency- and amplitude-modulated with double pass acousto-optic modulators, driven by a Signadyne arbitrary waveform generator. The two beams overlap on the memory crystal, a 0.05 % Pr^{3+}:Y_2SiO_5 sample of length $L = 5$ mm, located in a closed cycle cryostat operating at 3.5 K (Cryostation, Montana Instruments). The optical transition of interest for the storage of light, the $^3H_4(0) \rightarrow ^1D_2(0)$, is characterized by an inhomogeneous width of 6 GHz. After the storage, the retrieved signal is coupled in a polarization maintaining single-mode fiber and collected with a photodetector.

The first step in the preparation of the memory is to create a transparency window within the $^3H_4(0) \rightarrow ^1D_2(0)$ transition of Pr^{3+} by sweeping the laser by about 12 MHz [32]. This operation empties the $1/2_g$ and $3/2_g$ states of a given class of Pr^{3+} ions (see energy level scheme depicted in Fig. 1(a)). A narrower sweep is then operated outside the transparency window, to burn back a 2.1 MHz wide absorption feature at the frequency of the $1/2_g \rightarrow 3/2_e$ transition [22, 33]. This operation also fills the $3/2_g$ state, which should be empty for the spin-wave storage. Thus, a cleaning pulse resonant with the $3/2_g \rightarrow 3/2_e$ transition is sent to empty this ground state, but also to suppress the transitions of other classes of Pr^{3+} ions addressed by the burn-back pulses [34]. Finally, we burn a spectral hole with a sequence of single-frequency pulses on the single class absorption feature at the $1/2_g \rightarrow 3/2_e$ transition frequency. Simultaneously, we apply an additional train of short pulses to clean the

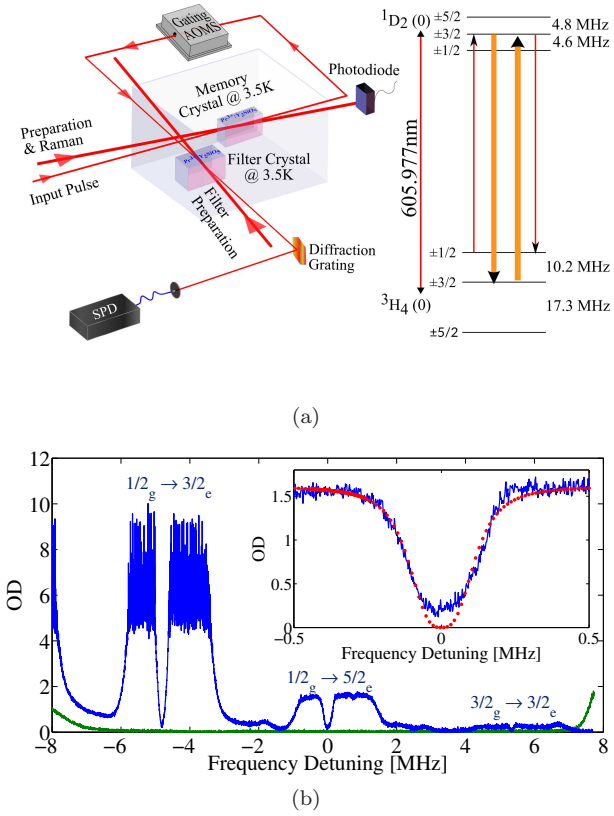

FIG. 1: (a) Left Panel: experimental setup. The preparation/Raman and input beams arrive at the memory with an angle of $\sim 4°$. The polarization is rotated along the D_2 crystal axis in order to maximize the absorption. For single-photon level measurements, weak coherent states are prepared by attenuating the input pulses with neutral density filters. Right Panel: hyperfine splitting of the first sublevels (0) of the ground $^3H_4$ and the excited $^1D_2$ manifold of Pr^{3+} in Y_2SiO_5. (b) Spectral holes burnt in 2 MHz-wide single class absorption features. Inset: magnification of the spectral hole resonant with the $1/2_g - 5/2_e$ transition. The fit of the hole shape with a *hyperlorentzian* function (see text for the details) is also shown.

anti-hole which rises at the frequency of the $3/2_g \rightarrow 3/2_e$ transition. The optical depth and the spectral width of the hole can be determined by choosing the proper combination of number, intensity and duration for the preparation pulses. The choice of the described preparation scheme with respect to a bare hole burning procedure within the inhomogeneous absorption profile [35] has a three-fold aim. It allows us to address only a single class of ions, to empty the spin storage state, and also to control the optical depth of the spectral hole, by varying the burn back power used to create the single class absorption feature. An example of absorption trace with spectral holes, about $\Delta_0 = 230$ kHz wide and of optical depth $\alpha L = 8.7$, burnt on single class absorption features is provided in Fig. 1(b). It is worth noting that, due to

a limited dynamical range of the photodetector, we cannot directly measure the optical depth of the spectral hole at the $1/2_g \rightarrow 3/2_e$ transition. We extrapolate the value by fitting the hole on the $1/2_g \rightarrow 5/2_e$ transition (shown in the inset of Fig. 1(b)), which is not affected by the detector non-linearity, and applying a scaling factor according to the relative oscillator strength of the two optical transitions [32]. The validity of our approach is tested by preparing weakly absorbing features and comparing the directly measured optical depth with the one extrapolated.

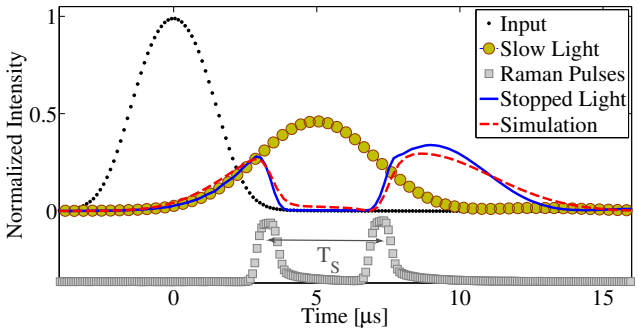

FIG. 2: The spectral hole memory scheme. Black dotted trace: input pulse; green solid circles: slowed pulse; blue solid trace: stopped light; grey square trace: Raman pulses (arbitrary units). The red dashed trace represents the numerical simulation of stopped light.

The light storage sequence is depicted in Fig. 2. An input pulse is sent resonantly to the spectral hole prepared in the $1/2_g \rightarrow 3/2_e$ transition. The Gaussian pulse has a duration of $3\,\mu$s (full width at half maximum, FWHM). The black dot trace in Fig. 2 represents the input pulse, linearly polarized perpendicular to the D_2 axis to minimize the absorption, traveling through a 18 MHz-wide transparency window. We assume it undelayed and take it as a reference. When the pulse penetrates through the spectral hole presented in Fig. 1(b), it is slowed down by approximately $5\,\mu$s (green solid circles in Fig. 2). The delayed pulse is stretched and slightly attenuated with respect to the Gaussian $3\,\mu$s input pulse because its bandwidth ~ 150 kHz FWHM is comparable to the more squarish hole width $\Delta_0 = 230$ kHz. A longer pulse would be less stretched but not sufficiently separated from the input for the spin storage step [31]. The situation represented in Fig. 2 is therefore a good trade-off.

The square-like shape of the hole is mostly due to imperfect locking of the laser leading to frequency jitter. To account for it, we fit the absorption profile by an *hyperlorentzian* function given by the equation

$$g(\Delta) = 1 - \frac{1}{1 + |2\Delta/\Delta_0|^n} \qquad (1)$$

($n = 2$ for a lorentzian), where Δ is the frequency detuning. From the fit, we obtain the previously mentioned values $\Delta_0 = 230$ kHz with $n = 3.0$ and $\alpha L = 8.7$ (see the red dashed trace in the inset of Fig. 1(b)).

We then transfer the optical collective excitation to a spin-wave using a short Raman pulse (grey square trace in Fig. 2) on the $3/2_e \rightarrow 3/2_g$ transition. After a controllable time T_s, a second Raman pulse triggers the pulse emission by reconverting the spin-wave into an optical excitation that will slowly propagate through the crystal. This is shown with the blue solid trace in Fig. 2. Since the delay of the slow light is not sufficient to completely compress the initial pulse into the crystal, some light escapes before we send the first Raman pulse. For this measurement, the storage and retrieval efficiency η_S, calculated as the ratio between the areas of the retrieved pulse (after the second Raman pulse) and the input pulse, is 39 %.

The pulse propagation and storage is modeled by the Schrödinger-Maxwell equations in one dimension (along z). For three-level atoms, the rotating-wave probability amplitudes C_g, C_e and C_s for the ground ($1/2_g$), excited ($3/2_e$) and spin ($3/2_g$) states, respectively, are governed by the time-dependent Schrödinger equation:

$$i\partial_t \begin{bmatrix} C_g \\ C_e \\ C_s \end{bmatrix} = \begin{bmatrix} 0 & \mathcal{E}/2 & 0 \\ \mathcal{E}/2 & -\Delta & \Omega/2 \\ 0 & \Omega/2 & 0 \end{bmatrix} \begin{bmatrix} C_g \\ C_e \\ C_s \end{bmatrix} \qquad (2)$$

where $\mathcal{E}(z,t)$ is the envelope of the input signal. As a consequence, C_g, C_e and C_s depend on z and t for a given detuning Δ within the inhomogeneous broadening. Raman pulses applied on the $3/2_e \rightarrow 3/2_g$ are described by the envelope $\Omega(t)$ which does not depend on z because the state $3/2_g$ is initially empty (no absorption). The Raman beam satisfies the two-photon resonance condition. We completely neglect the decoherence in this first approach since we are mostly interested in modeling the efficiency for storage times shorter than the coherence time.

The propagation of the signal $\mathcal{E}(z,t)$ is described by the Maxwell equation that can be simplified in the slowly varying envelope approximation:

$$\partial_z \mathcal{E}(z,t) + \frac{1}{c}\partial_t \mathcal{E}(z,t) = -\frac{i\alpha}{2\pi}\int_\Delta g(\Delta)\, C_g C_e^* \mathrm{d}\Delta \qquad (3)$$

The term $C_g C_e^*$ is the atomic coherence on the $1/2_g \rightarrow 3/2_e$ transition, proportional to the atomic polarization. The light coupling constant is directly included in the absorption coefficient α.

The Schrödinger-Maxwell equations (2,3) can be further simplified because the signal is weak. In the perturbative regime $C_g \simeq 1$, so the atomic evolution is only described by C_e and C_s.

Slow-light propagation (without Raman pulses) can be described with analytical expressions because in that case $C_s = 0$ thus reducing eq. (2) to the evolution of C_e only [35]. For the storage step (with Raman pulses), the

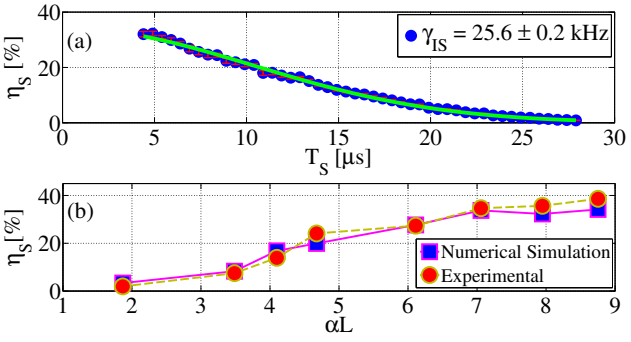

FIG. 3: (a) Storage efficiencies as a function of the delay T_s between the two Raman pulses. The decay is fitted with a Gaussian profile and the inhomogeneous spin broadening of $\gamma_{IS} = (25.6 \pm 0.2)$ kHz is extracted. (b) Storage efficiencies (experimental: red circles; numerical simulation: blue squares) as a function of the hole optical depth.

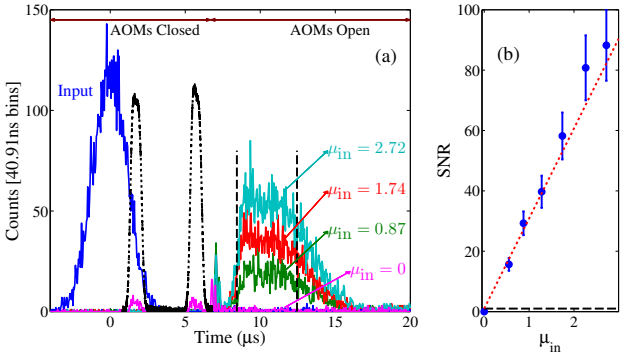

FIG. 4: (a) Time histograms of the retrieved photons measured for different input photon numbers when a spectral hole 350 kHz-wide is burnt in the memory crystal and a filtering window 1 MHz-wide is prepared in the filter crystal. The input with $\mu_{in} = 2.72$ (blue solid trace) and the Raman pulses (black dotted trace), as measured in photon counting and from a reference photodiode, respectively, are also displayed. The detection window $\Delta t_d = 4\,\mu$s is indicated by the dashed lines about the retrieved signal. (b) Signal-to-noise ratio as a function of the number of input photons. The error bars are evaluated with Poissonian statistics. The black dashed line indicates the limit of detection $SNR = 1$. The dotted line is a linear fit of the experimental data, from which the μ_1 value of 0.030 ± 0.004 can be obtained.

Schrödinger-Maxwell equations should be integrated numerically to reproduce the storage and retrieval of the input pulse when the Raman field $\Omega(t)$ is composed of two π-pulses. For a given inhomogeneous detuning Δ, we calculate the atomic evolution (2) by using a fourth-order Runge-Kutta method. After integrating over the inhomogeneous broadening using the *hyperlorentzian* function (1) for $g(\Delta)$, the propagation equation (3) is integrated along z using the Euler method. The stopped light temporal profile can be well reproduced by our numerical simulation (red dashed trace) in Fig. 2. To account for a possible imperfection of the Raman transfer to the spin state, we have adjusted the Raman pulse area to 0.85π instead of π. This artificially incorporates the decoherence mechanism that is not included in our model.

In order to characterize the storage, we investigate the efficiency of the stopped light as a function of the delay between the two Raman pulses, T_s, and of the hole optical depth by varying the power and duration of the preparation pulses. We show in Fig. 3(a) that the decay of the signal is compatible with the inhomogeneous broadening of the spin transition (with inhomogeneous linewidth $\gamma_{IS} = (25.6 \pm 0.2)$ kHz), confirming that the pulse energy is stored as a spin wave [20–22].

In Fig. 3(b) we compare the experimental values of storage efficiencies (red circles) and the results of the numerical simulations (blue squares) as functions of the optical depth αL. For these measurements, the position of the first Raman pulse is always optimized in order to maximize the efficiency since the group delay decreases at lower optical depths. We observe that the efficiency grows steadily as a function of optical depth. The experimental measurements are well reproduced by the numerical integration of the Schrödinger-Maxwell equations thus supporting our analysis.

In order to test the suitability of our optical memory to work in the quantum regime, we insert neutral density filters in the input mode to decrease the intensity of the input pulses down to the single-photon level. For these measurements, we perform 1000 storage and retrieval trials for each memory preparation, at a rate of 5 kHz. In order to discriminate the retrieved single-photon-level signals from the noise originated from the Raman pulses, we apply several filtering strategies (see Fig. 1(a)) [22]. First of all, the input and the preparation/Raman modes are spatially separated with an angle of about 4°. After the memory, the retrieved signal is first steered to two single pass AOMs acting as temporal gates. Then it is sent to a second Pr^{3+}:Y_2SiO_5 crystal where a narrow (1 MHz) transparency window is created at the input pulse frequency. Here, off-resonant Pr^{3+} ions are absorbing the noise at the Raman pulse frequency. The fluorescence not resonant with the Pr^{3+} $^3H_4(0) \rightarrow {}^1D_2(0)$ transition is then suppressed with a diffraction grating. Finally, the stored and retrieved light is detected with a single-photon detector (SPD). The total transmission of the input light from the cryostat window until the SPD is around 15 %. We record the arrival times of the photons and reconstruct the time histogram for different input photon numbers μ_{in}, as shown in Fig. 4. From the trace with $\mu_{in} = 0$, we measure an unconditional noise floor of $(9 \pm 1) \times 10^{-3}$ photons per pulse in a detection window $\Delta t_d = 4\,\mu$s. The storage and retrieval efficiencies are around 23 % for $\Delta t_d = 4\,\mu$s and 31% for $\Delta t_d = 7\,\mu$s. These are the highest efficiencies obtained

so far for solid state spin-wave optical memories at the single-photon level. Fig. 4(b) shows the behavior of the signal-to-noise ratio (SNR) of the retrieved photons as a function of μ_{in}. We measure a SNR of 33 ± 4 (23 ± 3) for $\mu_{in} = 1$ when $\Delta t_d = 4\,\mu$s ($\Delta t_d = 7\,\mu$s), the highest values measured so far for a single photon level solid state spin-wave memory [22, 23]. An important figure of merit for a single-photon-level optical memory is the parameter $\mu_1 = \mu_{in}/SNR$, which gives the minimum μ_{in} to reach a $SNR = 1$ for the retrieved photon. It has been shown that, in order to achieve quantum storage with a external single-photon source, a necessary condition is to have $p > \mu_1$, where p is the probability to find a single photon before the memory [22, 23]. From the slope in Fig. 4 (b), we find μ_1=0.030 ± 0.004. Our system is therefore very promising for quantum light storage, provided that μs-long single photons are available. Such long photons could be created from atomic ensembles [36] or single ions [37] and frequency shifted to the resonance frequency of the Pr^{3+} doped crystal by quantum frequency conversion techniques [33, 38, 39]. Shorter photons could also be stored if larger holes are prepared. However, in order to keep a sufficient separation between the second Raman pulse and the emitted photon, shorter Raman pulses should be used, which in turn will require a larger Rabi frequency. This could be achieved by increasing the Raman pulse power, or more efficiently by confining the interaction, e.g. in a waveguide configuration.

In our experiment, we store and retrieve single mode weak pulses while many applications require the storage and retrieval of photonics qubits. However, our protocol could be readily extended to the storage of polarization qubits [10, 11, 17] or to frequency-bin qubits [12, 40].

To conclude, we implemented a new light storage protocol based on stopped light in a spectral hole in a doped crystal and we achieved a storage and retrieval efficiency of up to 39 %. Thanks to a low unconditional noise floor, we store and retrieve single-photon-level pulses with high signal-to-noise ratio. This demonstrates that the memory can work in the quantum regime, with the highest efficiency so far obtained for spin-wave solid state optical memories. These results are promising for the realization of robust, highly efficient and long-lived spin-wave solid state quantum memories.

Acknowledgments. This work was supported by the People Programme (Marie Curie Actions) of the EU FP7 under REA Grant Agreement No. 287252.

Research at ICFO is supported by the ERC starting grant QuLIMA, by the Spanish Ministry of Economy and Competitiveness (MINECO) and the Fondo Europeo de Desarrollo Regional (FEDER) through grant FIS2012-37569.

Research at Laboratoire Aimé Cotton is supported by the French national grants ANR-12-BS08-0015-02 (RAMACO) and ANR-14-CE26-0037-02 (DISCRYS).

* Present address: Department of Physics, Clarendon Laboratory, University of Oxford, Oxford OX1 3PU, United Kingdom

† Electronic address: margherita.mazzera@icfo.es

[1] K. Hammerer, A. S. Sørensen, and E. S. Polzik, Rev. Mod. Phys. **82**, 1041 (2010).
[2] F. Bussières *et al.*, Journal of Modern Optics **60**, 1519 (2013).
[3] L.-M. Duan, M. D. Lukin, J. I. Cirac, and P. Zoller, Nature **414**, 413 (2001).
[4] N. Sangouard, C. Simon, H. de Riedmatten, and N. Gisin, Rev. Mod. Phys. **83**, 33 (2011).
[5] H. J. Kimble, Nature **453**, 1023 (2008).
[6] E. Knill, R. Laflamme, and G. J. Milburn, Nature **409**, 46 (2001).
[7] H. de Riedmatten *et al.*, Nature **456**, 773 (2008).
[8] I. Usmani, M. Afzelius, H. de Riedmatten, and N. Gisin, Nat Commun **1**, 12 (2010).
[9] M. Sabooni *et al.*, Phys. Rev. Lett. **105**, 060501 (2010).
[10] M. Gündoğan *et al.*, Phys. Rev. Lett. **108**, 190504 (2012).
[11] Z.-Q. Zhou *et al.*, Phys. Rev. Lett. **108**, 190505 (2012).
[12] N. Sinclair *et al.*, Phys. Rev. Lett. **113**, 053603 (2014).
[13] B. Lauritzen *et al.*, Phys. Rev. Lett. **104**, 080502 (2010).
[14] M. P. Hedges, J. J. Longdell, Y. Li, and M. J. Sellars, Nature **465**, 1052 (2010).
[15] C. Clausen *et al.*, Nature **469**, 508 (2011).
[16] E. Saglamyurek *et al.*, Nature **469**, 512 (2011).
[17] C. Clausen, F. Bussières, M. Afzelius, and N. Gisin, Phys. Rev. Lett. **108**, 190503 (2012).
[18] D. Rieländer *et al.*, Phys. Rev. Lett. **112**, 040504 (2014).
[19] E. Saglamyurek *et al.*, Nat Photon **9**, 83 (2015).
[20] M. Afzelius *et al.*, Phys. Rev. Lett. **104**, 040503 (2010).
[21] M. Gündoğan *et al.*, New Journal of Physics **15**, 045012 (2013).
[22] M. Gündoğan *et al.*, Phys. Rev. Lett. **114**, 230501 (2015).
[23] P. Jobez *et al.*, Phys. Rev. Lett. **114**, 230502 (2015).
[24] T. Chanelière *et al.*, Nature **438**, 833 (2005).
[25] M. D. Eisaman *et al.*, Nature **438**, 837 (2005).
[26] K. S. Choi, H. Deng, J. Laurat, and H. J. Kimble, Nature **452**, 67 (2008).
[27] S. Zhou *et al.*, Opt. Express **20**, 24124 (2012).
[28] A. V. Turukhin *et al.*, Phys. Rev. Lett. **88**, 023602 (2001).
[29] J. J. Longdell, E. Fraval, M. J. Sellars, and N. B. Manson, Phys. Rev. Lett. **95**, 063601 (2005).
[30] G. Heinze, C. Hubrich, and T. Halfmann, Phys. Rev. Lett. **111**, 033601 (2013).
[31] R. Lauro, T. Chanelière, and J.-L. Le Gouët, Phys. Rev. A **79**, 053801 (2009).
[32] M. Nilsson *et al.*, Phys. Rev. B **70**, 214116 (2004).
[33] N. Maring *et al.*, New Journal of Physics **16**, 113021 (2014).
[34] O. Guillot-Noël *et al.*, Phys. Rev. B **75**, 205110 (2007).
[35] R. Lauro, T. Chanelière, and J. L. Le Gouët, Phys. Rev. A **79**, 063844 (2009).
[36] L. Zhao *et al.*, Optica **1**, 84 (2014).
[37] A. Stute *et al.*, Nature **485**, 482 (2012).
[38] A. G. Radnaev *et al.*, Nat Phys **6**, 894 (2010).
[39] B. Albrecht *et al.*, Nat Commun **5**, (2014).
[40] L. Olislager *et al.*, Phys. Rev. A **82**, 013804 (2010).